Massively parallel assessment of gene regulatory activity at human cortical structure associated variants

Nana Matoba[1,2,*], Jessica C. McAfee[1,2,*], Oleh Krupa[1,2], Jess Bell[1,2,†], Brandon D. Le[1,2], Jordan M. Valone[1,2], Gregory E. Crawford[3], Hyejung Won[1,2,#], Jason L. Stein[1,2,#]

Affiliations:
[1] Department of Genetics, University of North Carolina at Chapel Hill; Chapel Hill, NC, USA
[2] UNC Neuroscience Center, University of North Carolina at Chapel Hill; Chapel Hill, NC, USA
[3] Department of Pediatrics, Duke University, Durham, NC, USA

[†] Current address: Department of Human and Molecular Genetics, Virginia Commonwealth University, Richmond, VA, USA
* These authors contributed equally: Nana Matoba, Jessica C. McAffee
# These authors jointly supervised this work: Hyejung Won, Jason L. Stein

Corresponding authors
Correspondence to Hyejung Won (hyejung_won@med.unc.edu) or Jason L. Stein (jason_stein@med.unc.edu)

Abstract

Genetic association studies have identified hundreds of largely non-coding loci associated with inter-individual differences in the structure of the human cortex, though the specific genetic variants that impact regulatory activity are unknown. We implemented a Massively Parallel Reporter Assay (MPRA) to measure the regulatory activity of 9,092 cortical structure associated DNA variants in human neural progenitor cells during Wnt stimulation and at baseline. We identified 918 variants with regulatory potential from 150 cortical structure associated loci (76% of loci studied), of which >50% showed allelic effects. Wnt stimulation modified regulatory activity at a subset of loci that functioned as condition-dependent enhancers. Regulatory activity in MPRA was largely induced by Alu elements that were hypothesized to contribute to cortical expansion. The regionally specific impact of genetic variants that disrupt motifs is likely mediated through the levels of transcription factor expression during development, further clarifying the molecular mechanisms altering cortical structure.

Main

Introduction

The expansion of the cerebral cortex in humans, relative to non-human primates, is thought to contribute to our distinctive cognitive and social abilities[1,2]. Genetic association studies conducted in large consortia, including the Enhancing Neuroimaging Genetics through Meta-analysis (ENIGMA), have identified single nucleotide polymorphisms (SNPs) associated with inter-individual variability in human cortical surface area and thickness measured with magnetic resonance imaging, providing a foothold into the molecular mechanisms affecting human cortical size and shape[3]. However, most cortical structure associated variants are found in non-coding regions of the genome without a clearly defined function.

Cortical structure associations are enriched in regulatory regions of the genome active in primary human neural progenitor cells (phNPCs) and colocalize with genetic variants influencing chromatin accessibility - a proxy for transcription factor (TF) binding - and gene expression specifically in NPCs (chromatin accessibility and expression quantitative trait loci; ca/eQTLs)[3–6]. This suggests cortical structure associated variants alter gene regulatory elements by modifying TF binding and gene expression, impacting fate decisions of phNPCs during prenatal development, ultimately leading to differences in cortical size in adulthood. TFs exhibit regionally specific expression patterns[7], and translocate to the nucleus in response to activation of developmental signaling pathways such as Wnt[8], which may lead to variants having stronger or weaker effects within specific regions or in stimulated conditions. This hypothesis is supported by cortical structure associations enriched within Wnt responsive regulatory elements and associations found near genes involved in the canonical Wnt pathway[3,6].

Gene regulatory elements are marked by accessible chromatin or histone post-translational modifications that allow TF binding, and through looping with promoters, can influence gene expression[9–12]. In addition to chromatin loops, enhancer RNAs (eRNAs), transcribed in non-coding genomic regions, initiate looping through complementarity to upstream antisense promoter RNAs (uaRNAs) recruiting polymerase to increase transcription[13,14]. The latter mechanism involves co-opting the expression of Alu elements, a set of transposable elements that are prevalent across the human genome[15]. Alu elements have been theorized to strongly contribute

67 to human cortical evolution because they have increased in prevalence together with brain size
68 along the human lineage[16].
69
70 Due to the correlation of nearby genetic variants (linkage disequilibrium or LD), the specific
71 variant(s) with gene regulatory activity in an associated locus are unknown. We implemented a
72 Massively Parallel Reporter Assay (MPRA), a high-throughput experiment designed to measure
73 the regulatory activity of short DNA sequences using barcoded expression constructs to identify
74 cortical structure associated variants with gene regulatory activity[17,18]. MPRA can measure the
75 regulatory function of a given element (MPRA activity) as well as the influence of an allele within
76 the regulatory element (allelic effect or expression modulating variant [emVar]). Here, we tested
77 the regulatory impact of 9,092 cortical structure associated variants within phNPCs. Considering
78 the role of the Wnt signaling pathway in brain size[19], we tested whether regulatory potential of
79 variants changes in response to Wnt stimulation. We identified 1,258 elements (7% of elements
80 tested) with regulatory potential from 150 cortical structure associated loci (76% of loci studied).
81 Among these, >50% of cortical structure associated variants showed allelic effects. Regulatory
82 activity in MPRA was largely driven by Alu elements, a small subset of which showed condition-
83 dependent gene regulatory function. Disruption of motifs by emVars highlighted TFs likely
84 involved in human brain development and suggested that the impact of genetic variants on
85 different brain regions is mediated by levels of TF expression in those regions. Overall,
86 characterization of MPRA-validated cortical structure associated variants further clarify molecular
87 mechanisms altering cortical structure.
88

Results

MPRA design and reproducibility

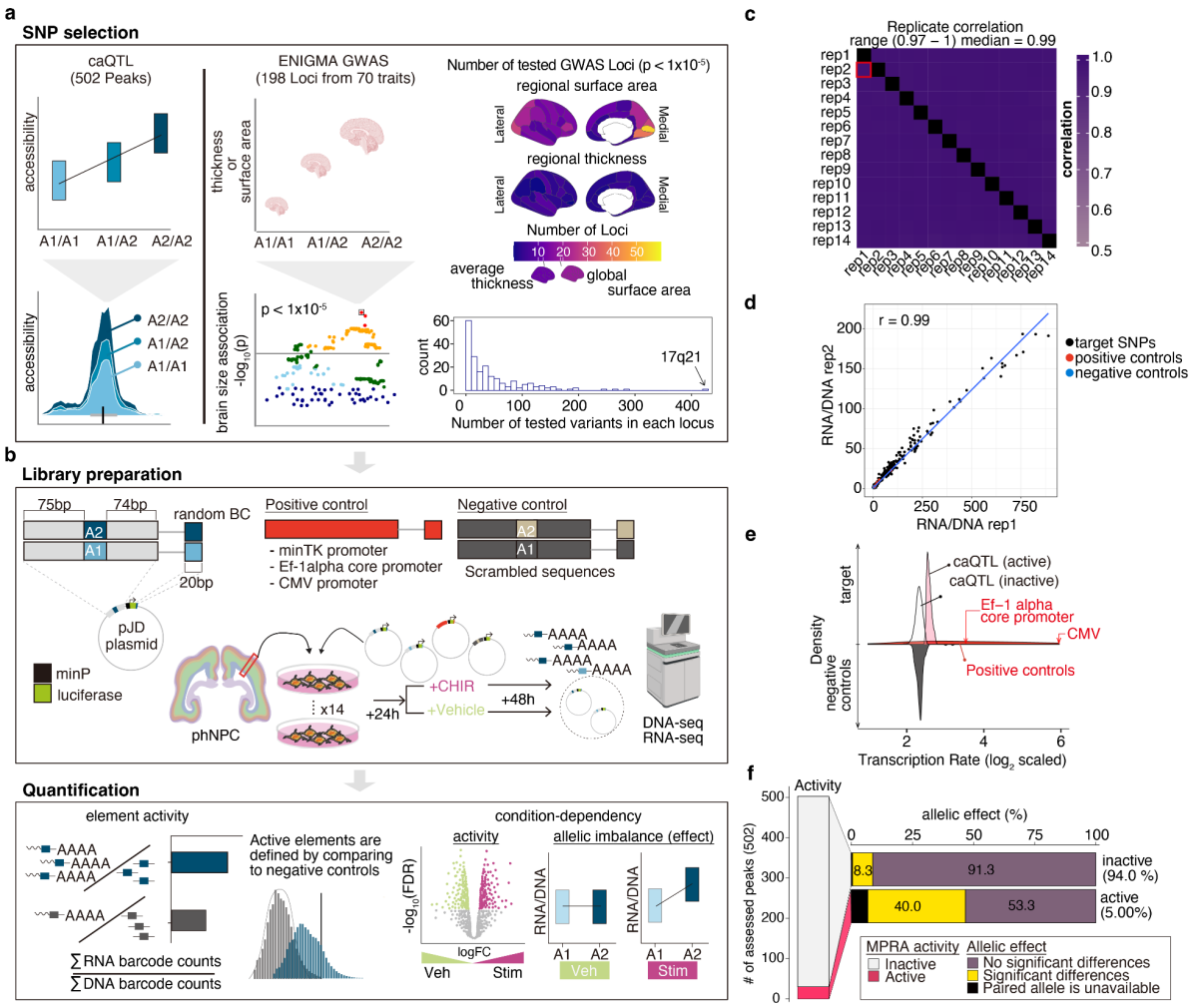

Fig.1 Experimental design and reproducibility

a, SNP selection. 502 caQTLs were chosen in chromatin accessible peaks in phNPCs (left). ENIGMA GWAS data contains SNPs associated with surface area or thickness (global and 34 regions of the cortex) (right). Cortical regions are color-coded according to the number of loci included in this study, stratified by surface area and thickness (top) and the number of elements per locus (bottom). **b**, Experimental design. **c**, Replicate correlations of MPRA activity were uniformly strong (median = 0.99). **d**, An example correlation of MPRA activity across two replicates. Each set of MPRA elements is colored along with a line of best fit. **e**, Histograms of MPRA activity, quantified as transcription rate, for different sets of MPRA elements, where positive controls showed higher MPRA activity than negative controls (see also **Supplementary Fig. 4**). For visualization purposes, the distribution of negative controls are shown upside down. **f**, MPRA activity of caQTL elements above the negative controls

102 (MPRA active; FDR < 0.1) was detected in either allele of 37 regions from 502 assessed. Allelic
103 expression imbalances (allelic effects) were observed more frequently in MPRA active elements.
104
105
106 We designed four sets of 150 base pair elements to understand the gene regulatory and allelic
107 effects governing human brain development and structure (**Fig. 1a,b**): (1) *positive controls*: 10
108 constitutively active promoter regions commonly used to drive transgene expression (min-tk
109 promoter, Ef1-alpha core promoter, CMV promoter) (2) *caQTLs*: 502 chromatin accessibility
110 peaks that contain bi-allelic SNPs replicably associated with their accessibility in a population of
111 phNPCs[4,6] (**Supplementary Fig. 1**), (3) *ENIGMA GWAS*: 9,092 regions centered on any SNP
112 associated ($P < 1 \times 10^{-5}$) with inter-individual differences in human cortical structure from 198
113 genome-wide significant loci[3] and (4) *negative controls*: 194 scrambled elements from the
114 ENIGMA GWAS. In total, we tested the regulatory activity of 19,500 elements.
115
116 Each element was synthesized and cloned into a plasmid upstream of a minimal promoter to drive
117 expression of luciferase followed by a random 20 bp barcode[20]. We transfected the pooled MPRA
118 library into 16 biological replicates of phNPCs. After 24 hours to allow expression of the MPRA
119 constructs, we activated Wnt signaling using CHIR (CHIR99021, also known as CT99021), a
120 potent GSK3β inhibitor and Wnt activator, or studied baseline gene regulation using a vehicle
121 (DMSO), for 48 hours[3,8,21]. For each biological replicate, we measured the expression of barcodes
122 using RNA-seq and the number of barcodes present in that replicate using DNA-seq. We
123 calculated the MPRA activity of an element as the summed RNA counts divided by the DNA
124 counts[20,22].
125
126 After removing outliers in expression level and filtering poorly represented elements (**Methods**,
127 **Supplementary Fig. 2**), we retained 28 (s.d. = 12.5) barcodes on average for each element
128 across 14 replicates (**Supplementary Fig. 3**). Regulatory activity was strongly correlated between
129 biological replicates, demonstrating the reproducibility of our assay (median Pearson's correlation
130 = 0.99; **Fig 1c,d**). At least one element from each positive control region showed significantly
131 higher regulatory activity than negative controls (Benjamini-Hochberg (BH)-adjusted *P*-value
132 [FDR] < 0.1; **Fig. 1e, Supplementary Fig. 4**), as expected.
133
134 We next evaluated the concordance between caQTLs from our previous work[4,6] and MPRA
135 conducted in the same cell type - phNPCs (**Supplementary Tables 1,2)**. Though there was
136 limited concordance between MPRA activity or allelic effects in caQTLs and MPRA, as found in

previous work[23–27] (**Supplementary Fig. 5**), the strongest predictor of detecting MPRA allelic effects from caQTLs was MPRA activity (Odds Ratio [O.R] = 8.22; two-sided Fisher's Exact test $P = 3.2 \times 10^{-6}$, **Fig. 1f, Supplementary Table 2**). Our subsequent downstream analyses only evaluated allelic effects when at least one allele showed MPRA activity significantly above negative control samples.

Identifying regulatory elements associated with inter-individual differences in human cortical structure

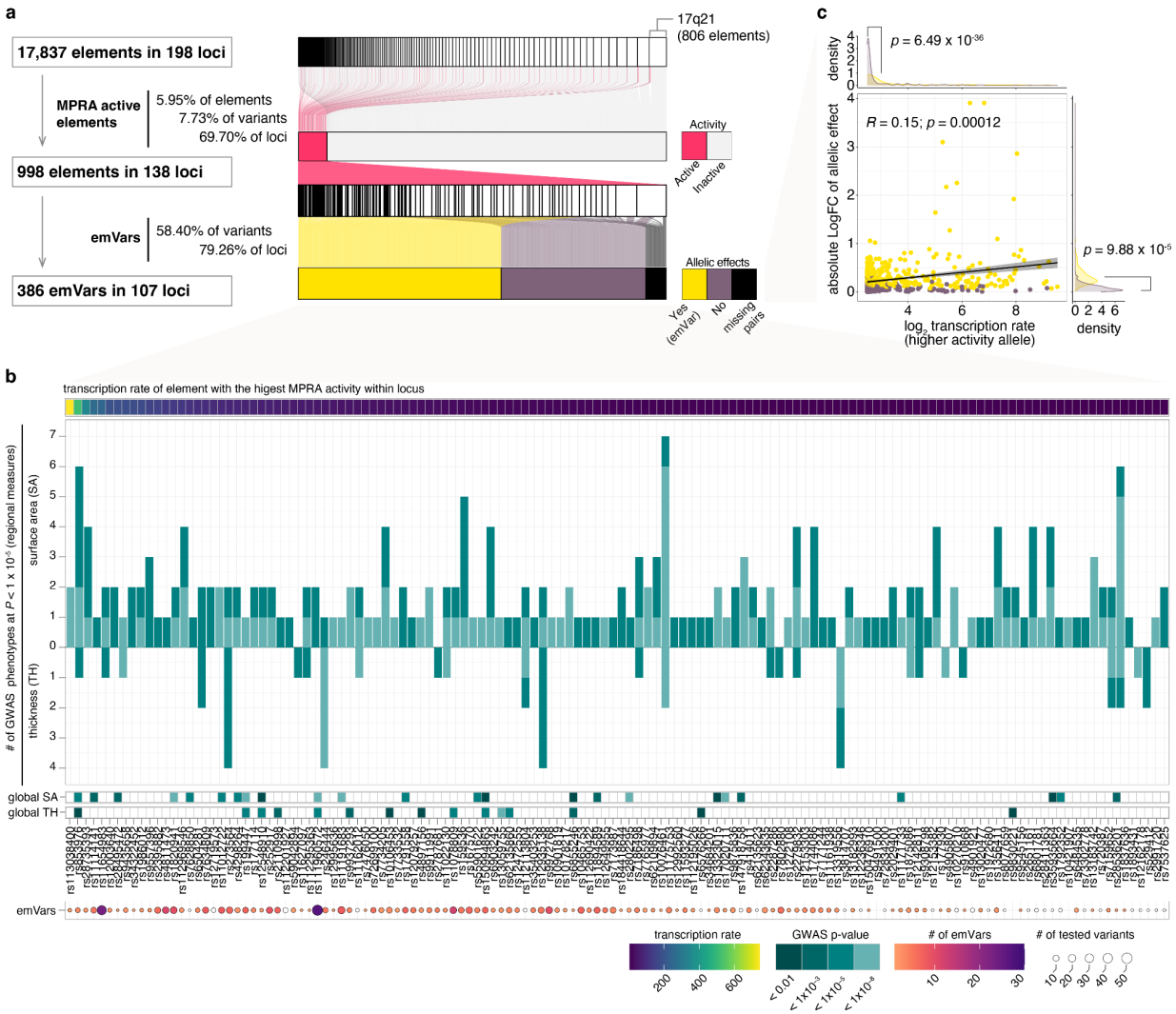

Fig. 2 MPRA regulatory activity and allelic effects at cortical structure associated loci

a, Summary of MPRA elements at cortical structure associated loci with MPRA activity and allelic effects. Sankey diagram illustrates the composition of elements across tested loci (top), colored by MPRA activity (middle) or emVars (bottom). emVars were tested only for variants where at least one allele showed MPRA activity. **b,** MPRA active cortical structure associated loci ordered by MPRA activity. *Top row:* the level of MPRA activity of the allele with highest activity within a locus. *Middle row:* a barplot showing the number of cortical regions (among 34) that were associated to a locus containing an MPRA active element colored by GWAS significance level, followed by GWAS *P-value* of global surface area and thickness. *Bottom row:* the number of emVars at the locus. **c**, MPRA transcription level of the higher activity allele is associated with the absolute value of allelic difference (logFC). The line was fitted using linear regression and shadows indicate 95% confidence interval. Pearson correlation coefficient (R) and its *P*-value are shown.

To identify cortical structure associated regulatory elements, we empirically tested the regulatory activity of genetic variants associated with inter-individual variability in human cortical structure from the ENIGMA GWAS[3] (**Fig. 1a, Supplementary Table 3a**). Cortical regions varied in the number of detected GWAS significant loci (e.g., 54 loci associated with pericalcarine surface area), and the number of associated SNPs within a locus due to LD patterns (e.g., 428 variants were tested at the large chromosome 17q21 inversion region[28]), influencing the number of elements tested in our MPRA (**Fig. 1a, Supplementary Table 3a**). The vast majority (88.4%) of variants tested in the MPRA were located in introns or intergenic regions, with presumed gene regulatory function. Twenty percent of variants were associated with both cortical surface area and thickness, suggesting these variants have pleiotropic effects (**Supplementary Fig. 6a, Supplementary Table 3a**).

Among 17,837 elements (9,052 variants) in 198 loci, we observed 988 elements with MPRA activity significantly higher than the negative controls in the vehicle condition (FDR < 0.1, **Fig. 2a**,**b**, **Supplementary Fig. 6**, **Supplementary Tables 1,3a**). While only 6% of tested elements showed MPRA activity, 70% of loci contained at least one element with detectable regulatory activity. This suggests that most cortical structure associated loci have at least one SNP with detectable regulatory activity in phNPCs using MPRA.

More MPRA active elements were discovered at surface area associated loci than at thickness associated loci, likely due to the larger number of elements tested for surface area (**Supplementary Fig. 6**). MPRA active elements generally had regionally limited effects, being significantly associated with only one or two cortical regions (GWAS $P < 1x10^{-5}$) rather than having broad impacts across the entire cortex (**Fig. 2b, Supplementary Fig. 6, Supplementary Table 3a**).

We next evaluated allelic effects at cortical structure associated loci that showed MPRA activity when both alleles were present. We found 386 variants with significant allelic effects (79% of loci, 58% of variants tested; FDR < 0.1; **Fig. 2b, Supplementary Tables 1,3b**), indicating that most cortical structure associated loci have at least one genetic variant capable of altering transcription in progenitor cells during brain development. Consistent with the caQTL dataset, emVars exhibited higher expression levels than non-emVars, further supporting the relationship between MPRA expression strength and allelic effects (**Fig. 2c**).

Cortical structure associated MPRA active elements are enriched in promoter regions of Alus

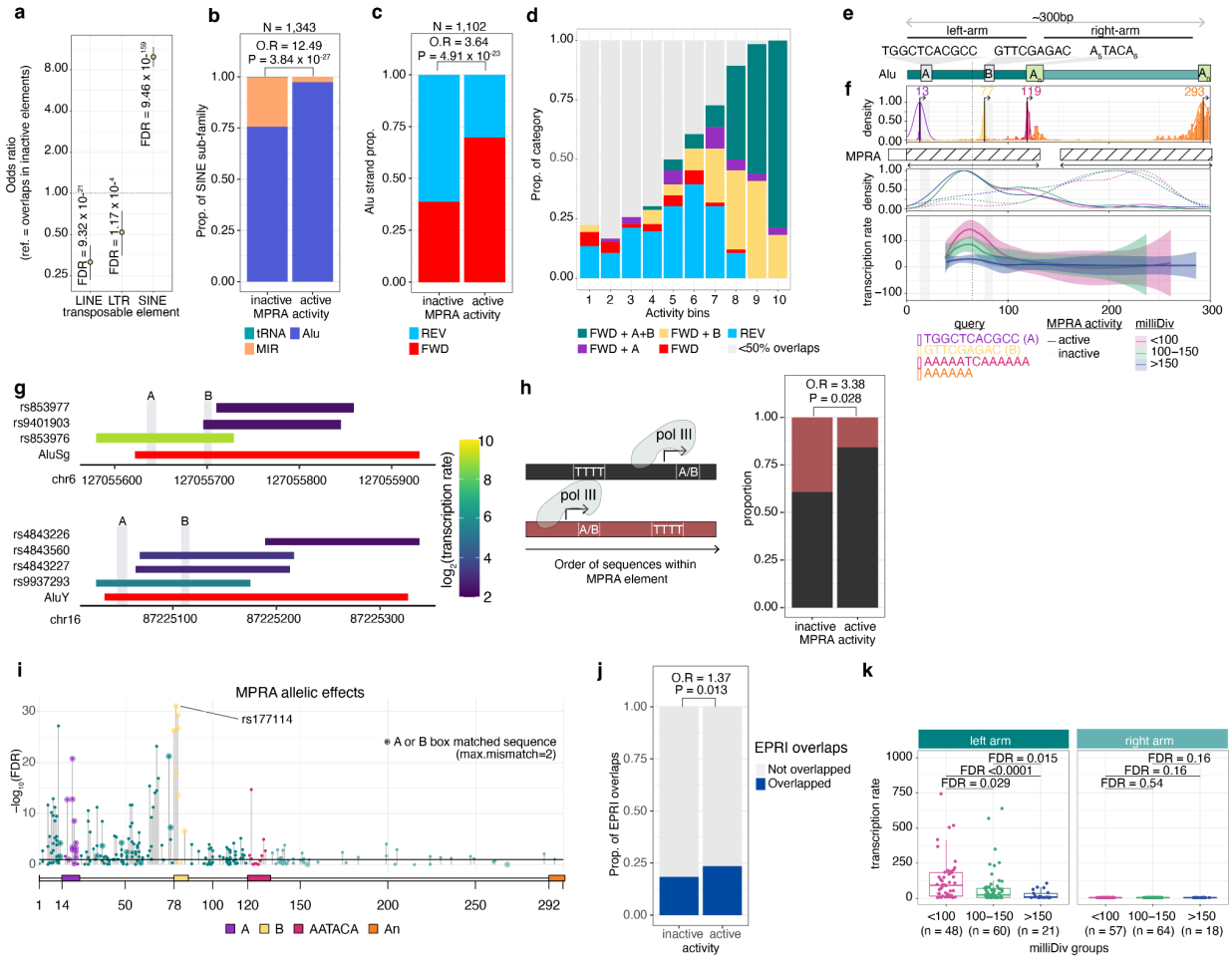

Fig. 3 MPRA activity of cortical structure associated loci is driven by Pol III promoter elements within Alus

a, Enrichment of MPRA active elements across classes of transposable elements, **b**, SINE-subfamily elements, and **c,** Alu element orientation, showing that forward Alu elements are major drivers of MPRA activity. **d,** MPRA active elements binned by level of activity were colored based on their overlap to Alu elements in different orientations (FWD/REV) or containing A and B box Pol III promoter elements. **e,** Schematic structure of a typical Alu-element which contains a left arm serving as Pol III promoter containing A and B boxes, followed by a right arm terminating with a polyA repeat. **f,** Frequency of MPRA elements containing sequence corresponding to the positions of observed consensus elements in the Alu element, including A and B boxes (top). Density of MPRA elements stratified by MPRA activity group across position (middle). Activity level of MPRA active elements graphed according to their position within the Alu element, stratified and colored using base mismatches in parts per thousand (milliDiv) (bottom). **g,** Example MPRA elements demonstrating that higher MPRA activity (color) is observed when the elements contain both A and B boxes. **h,** Elements where A/B matched sequences occur before the Pol III termination sequence (TTTT) are more often inactive. **i,** Significance of MPRA allelic effects mapped within the Alu element show that genetic variation near A/B boxes have strong effects on MPRA activity. **j,** Overrepresentation of MPRA active elements within enhancer RNAs or upstream antisense RNAs assessed in neural progenitor cells using RIC-seq[13]. **k,** Younger elements with lower milliDiv show higher activity than older elements, specifically when found in the left arm of the Alu element. Statistical significance of enrichment was assessed by two-sided Fisher's exact test. *P*-values were corrected for multiple comparisons using the Benjamini–Hochberg method. FWD: Forward, REV: Reverse, Veh: vehicle, O.R: odds ratio, EPRI: enhancer-promoter RNA interaction.

We next aimed to identify genetic features associated with MPRA active elements linked to cortical structure. We found that MPRA active elements were enriched in short interspersed nuclear elements (SINEs; 56.7% in active, 11.6% in inactive elements), consistent with previous MPRA experiments in other cell types[27,29] and phNPCs[20] (**Fig. 3a**). SINEs are a type of the retrotransposons comprising a set of DNA elements that express themselves and re-integrate into new positions, resulting in a large number of repeated copies found throughout the genome. Retrotransposons have been hypothesized to contribute to the rapid evolution of both gene regulation and human brain structure[16,30]. Among subfamilies of SINEs[31], MPRA active elements were specifically enriched in forward oriented Alu elements[32] (**Fig. 3b-d**), which aligned with our oligo design that used only forward sequences.

A typical Alu element contains two consensus sequences in its left arm that function as RNA polymerase III (Pol III) promoters, the A-Box (TGGCTCACGCC) and the B-Box (GTTCGAGAC)[33,34] (**Fig. 3e**). We estimated the relative position of MPRA elements within the Alu sequence, and observed that the most active MPRA elements were located in the left arm of the Alu element and contained the A or B boxes (**Fig. 3d-g**). Presence of both A and B boxes resulted in the highest MPRA activity (**Fig. 3d-g**). One of the scrambled sequences (negative control)

237 unintentionally contained a B-box like sequence (GTTCGAGC) and had strong MPRA activity,
238 further supporting that these Alu based sequences drive MPRA activity (**Supplementary Fig. 7**).
239 We also found reduced MPRA activity when elements containing A or B boxes were followed by
240 a TTTT (T4), the termination signal for Pol III (**Fig. 3h**). Subsequently, we explored allelic effects
241 within MPRA active elements that contained Alu sequences. We found that emVars were more
242 often found in Alu elements compared to MPRA active variants without allelic effects (O.R = 1.56,
243 P = 0.007). Notably, the variants with the most significant allelic effects on transcription were
244 located within the left arm of the Alu element and overlap or were close to A or B boxes, further
245 supporting the critical regulatory role of these regions (**Fig. 3i**).
246
247 Strong Alu-element driven transcription may be an artifact of non-chromatinized sequences in the
248 episomal MPRA library, that are normally silenced in the endogenous genome. We found that
249 MPRA active elements were enriched with eRNAs and uaRNAs in phNPCs[13] compared to MPRA
250 inactive elements (**Fig. 3j**), suggesting that at least a subset of MPRA active elements exhibit
251 endogenous genome activity.
252
253 The age of Alu elements can be estimated based on their accumulated mutations over time, with
254 younger Alu elements having lower sequence divergence to ancestral sequences than older Alu
255 elements. The level of sequence divergence can be measured using mismatches per thousand
256 bases to consensus sequences (milliDiv)[35]. We found that younger cortical structure associated
257 Alu elements (<100 milliDiv) showed higher activity than older elements (>150 milliDiv) (**Fig. 3f,k**),
258 consistent with previous findings[32]. These results suggest that more recent insertion of Alu
259 elements created novel gene regulatory regions impacting neurodevelopmental genes that
260 influenced cortical structure along the human lineage.
261
262 Overall, these results demonstrate that MPRA activity of cortical structure associated sequences
263 in neural progenitors are strongly driven by Alu elements, especially younger Alu, that enhance
264 Pol III based transcription.

Transcription factors contributing to regulatory function at cortical structure associated elements

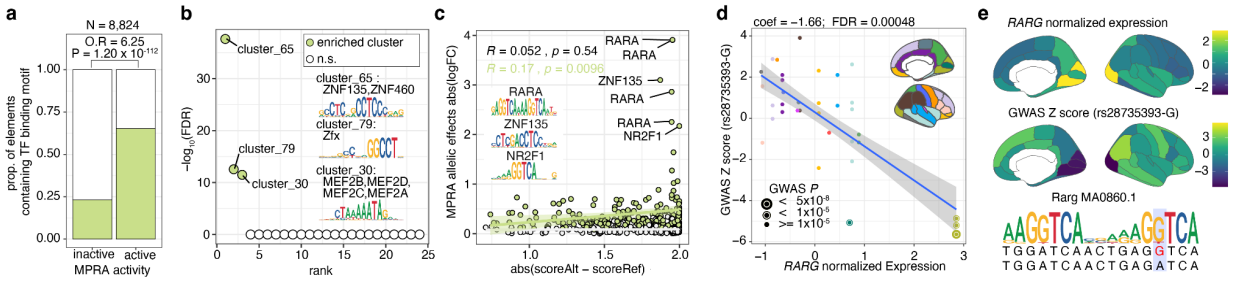

Fig. 4 TFs enriched in cortical structure associated regulatory elements and underlying regional specificity

a, Proportion of elements containing TF binding motifs stratified by MPRA activity. **b,** Enriched TF binding clusters. Statistical significance of enrichment in **a** and **b** were assessed by a two-sided Fisher's exact test. **c**, The level of TF motif disruption (x-axis) is related to MPRA allelic differences (y-axis). *P*-values were estimated by Pearson's correlation test. **d-e,** TF expression levels during prenatal development across brain regions (colored) were associated with the impact of variant on cortical structure. Each dot represents DK-atlas brain area colored by macro-scale brain area (**d**) (**Supplementary Fig. 8**). **e**, Brain areas are colored by scaled expression values (top) and GWAS Z-scores (middle). Seqlogo showing G allele matches the Rarg binding motif site (bottom). In **c** and **d**, the lines were fitted using linear regression and shadows indicate 95% confidence interval. *P*-values were corrected for multiple comparisons using the Benjamini–Hochberg method (**b,d**). O.R: odds ratio.

Since TF binding is known to regulate gene expression, we explored whether certain TF binding motifs contribute to MPRA activity. Elements with MPRA activity had more complex sequences as evaluated by Shannon entropy[36] ($p = 4.58 \times 10^{-24}$ using a t-test) and were more likely to contain a TF binding motif (**Fig. 4a**), as has been found in previous MPRA studies[22,25,37]. Specifically, three separate clusters of similar TF binding motifs (TFBMs) – ZNF135/460, MEF2A-D, and Zfx – were enriched in human cortical structure associated MPRA active elements in phNPCs (**Fig. 4b**). ZNF460 TFBMs were previously found to be enriched in great ape-specific structural variants and hypothesized to increase brain size along the human lineage[38]. Conditional knockout of *Mef2c* in mice was shown to reduce whole brain size[39]. *MEF2C* is also involved in neuronal differentiation, and genetic variation within or near this gene creates risk for psychiatric disorders[22,40]. Alu elements contain sequences similar to ZNF135, ZNF460, and MEF2A binding motifs which exhibit human-specific activity and may be driving this observed overlap[41,42].

294 Previous studies have shown that the level of motif disruption is associated with MPRA allelic
295 effects[22,37], so we evaluated this relationship in our data. We found that emVars strongly
296 correlated with the predicted level of motif disruption, whereas elements without allelic effects had
297 no detectable relationship with motif disruption (**Fig. 4c**). Our results suggest that TF binding
298 affinity impacts the strength of allelic effects on transcription observed in MPRA. Notably,
299 disruption of RARA, ZNF135, and NR2F1 motifs led to the largest impacts on MPRA activity. It
300 was reported that the consensus sequences of evolutionary recent Alu subfamiles contain binding
301 sites for retinoic acid receptors[43], consistent with our finding of stronger MPRA activity within
302 younger Alu elements (**Fig. 3f,k**). This indicates TFs that may shape the human cortex during
303 development.

304 Spatial relationships between TF expression and allelic effects

305 Genetic variants often are associated with differences in a limited number of cortical regions rather
306 than having global effects across all cortical regions, despite the fact that the variants are constant
307 in all cells (**Fig. 2b**). We hypothesized that the molecular mechanism underlying regionally specific
308 cortical structure effects is that regions more affected by a given variant would also have higher
309 expression of TFs disrupted by that variant, similar to findings from previous studies[44,45].
310 To test this hypothesis, we compared predicted TF binding motifs disrupted by emVars to
311 corresponding TF expression levels across 16 macroscale brain regions (**Supplementary Fig. 8**)
312 from 8 to 24 post-conception weeks (pcw) from the BrainSpan Atlas[46]. We then analyzed the
313 spatial correlation between TF expression and the impact of the variant on cortical structure[3]. We
314 found a significant correlation between GWAS effect sizes for 7 cortical structure associated
315 SNPs and regional TF expression (**Supplementary Tables 4,5**). For example, elevated *RARG*
316 expression was associated with a greater reduction in surface area in the presence of
317 rs28735393-G, which matches the Rarg binding motif (**Fig. 4d,e**). Our results suggest that TF
318 expression levels, in combination with genetic variants disrupting TF binding, modulate the impact
319 of genetic variants on cortical structure.
320

Wnt activity modulating MPRA activity

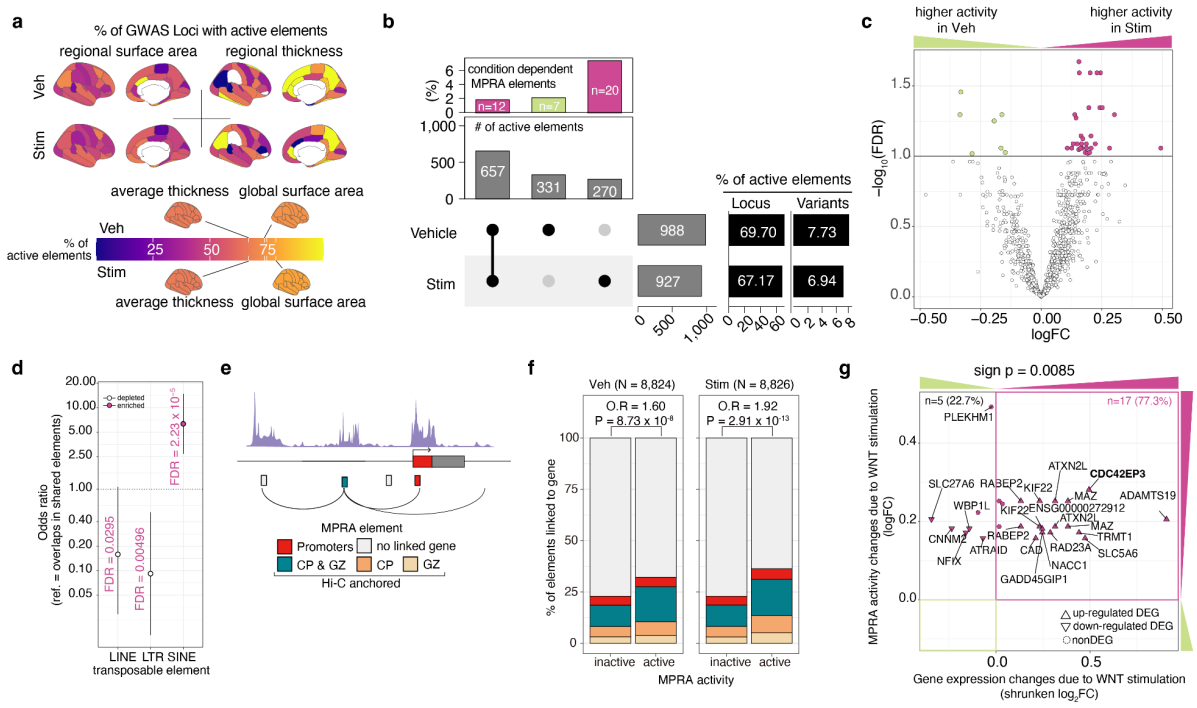

Fig. 5 Regulatory elements associated with cortical structure show condition-dependent function

a, The percentage of MPRA active elements across brain regions stratified by condition (top: Vehicle, bottom: Wnt Stimulation via CHIR) and measurement (left: surface area, right: thickness). **b,** The number of MPRA active elements in each condition (bottom). The top panel shows the percentage of condition-dependent MPRA elements. **c,** Volcano plot showing condition-dependent MPRA activity in Wnt stimulation vs vehicle. **d,** Enrichment of TEs within elements exhibiting higher activity during Wnt stimulation compared to elements without detectable differences in MPRA activity across stimulation conditions. **e,** Schematic example linking MPRA element to genes at their promoter region or using chromatin interaction (Hi-C) for distal elements. **f,** Percentage of MPRA elements linked to genes stratified by MPRA activity and condition. Active elements were more likely to be linked to a gene. **g,** Scatter plot showing gene expression changes

vs MPRA activity changes due to Wnt stimulation. A sign test was used to determine if condition-dependent MPRA activity occurred in the same direction as condition-dependent gene expression more than expected by chance. **h**, *CDC42EP3* locus highlighting a condition-dependent MPRA element (rs4670759). Top: -log10(p-value) from GWAS of inferior temporal cortex surface area. Each dot represents variants in the locus colored by LD (r^2) to the index SNP (rs9309013, purple diamond). Middle: $-\log_{10}$(FDR) of MPRA activity in stimulation or vehicle conditions. Bottom: Differential chromatin accessible peaks colored by shrunken log2FC, followed by a promoter region. **i-l,** Boxplots displaying differences between conditions in multiple measurements: MPRA activity (**i**), chromatin accessibility (**j**), gene expression (**k**) in phNPCs. **l,** MPRA allelic effects of rs4670759 in stimulated condition. Dots indicate replicates/donors in **i-l**. Same replicate was connected by line in **l**. ; *n* of replicates/donors: $n_{\text{MPRA}} = 14$, $n_{\text{chromatin_accessibility}} = 72$, $n_{\text{gene_expression}} = 74$. *P*-values were corrected for multiple comparisons using the Benjamini-Hochberg procedure. Stim: Stimulation, Veh: Vehicle, CP: cortical plate of the developing cortex; GZ: germinal zone of the developing cortex.

Wnt stimulation alters gene regulation to modulate proliferation and differentiation of NPCs shaping brain structure[6,8,19]. To evaluate the condition-dependent activity of cortical structure associated variants, we stimulated the Wnt pathway in phNPCs using CHIR (**Methods**). We detected a similar number of MPRA active elements (927 among 17,848 elements; 6.94% of tested variants and 67.17% of tested loci) in the stimulated condition (**Fig. 5a**,**b**, **Supplementary Fig. 6**, **Supplementary Tables 1,3c)**. The same TF clusters were enriched in MPRA active elements under both the vehicle and Wnt stimulated conditions, likely due to 657 active elements being detected in both conditions (**Supplementary Fig. 9**). While we detected 270 elements that were active only in the Wnt stimulated condition (**Fig. 5b**), many of these regions are likely just above or below the threshold cutoff. To more stringently evaluate condition dependency, we further identified MPRA active elements with significantly different levels of activity across conditions. We found 32 elements with higher activity due to Wnt stimulation and 7 elements with higher activity in the vehicle condition, demonstrating Wnt-dependent gene regulation of cortical structure associated elements (**Fig. 5b,c, Supplementary Table 3d**). MPRA active elements with higher activity in simulated conditions more often overlapped with SINEs compared to elements whose activity did not significantly differ between conditions (**Fig. 5d**).

Condition-dependent regulation of gene expression

In order to determine downstream impacts of condition-specific MPRA active elements, we mapped them to putative target genes. MPRA active elements in gene promoters were directly assigned to their target genes, while the rest were mapped to the target genes via chromatin interaction profiles in the developing brain[10]. We found that MPRA active elements were more

372 likely to be linked to a gene than MPRA inactive elements (**Fig. 5e, f**). Interestingly, elements with
373 increased MPRA activity under Wnt stimulation were linked to genes with higher expression under
374 the same condition[6], suggesting these elements function as condition-dependent enhancers[6] (**Fig.**
375 **5g**). As an example, rs4670759, a SNP associated with the surface area of the inferior temporal
376 cortex, showed higher MPRA activity (**Fig. 5h**) and increased chromatin accessibility (**Fig. 5i,j**)
377 under Wnt stimulation. This variant is located in the promoter of *CDC42EP3* (**Fig. 5h**), which is
378 involved in actin cytoskeleton formation[47] and whose expression is increased under Wnt
379 stimulation[6] (**Fig. 5k**). We note this element is an emVar in the stimulated condition, though we
380 were unable to test for allelic effects in the vehicle condition because one of the alleles was
381 missing in the QCed dataset (**Fig. 5l**). In summary, we present evidence that condition-dependent
382 MPRA activity of cortical structure associated SNPs results in condition-dependent effects on
383 gene expression.
384

Condition-dependent allelic effects at cortical structure associated loci

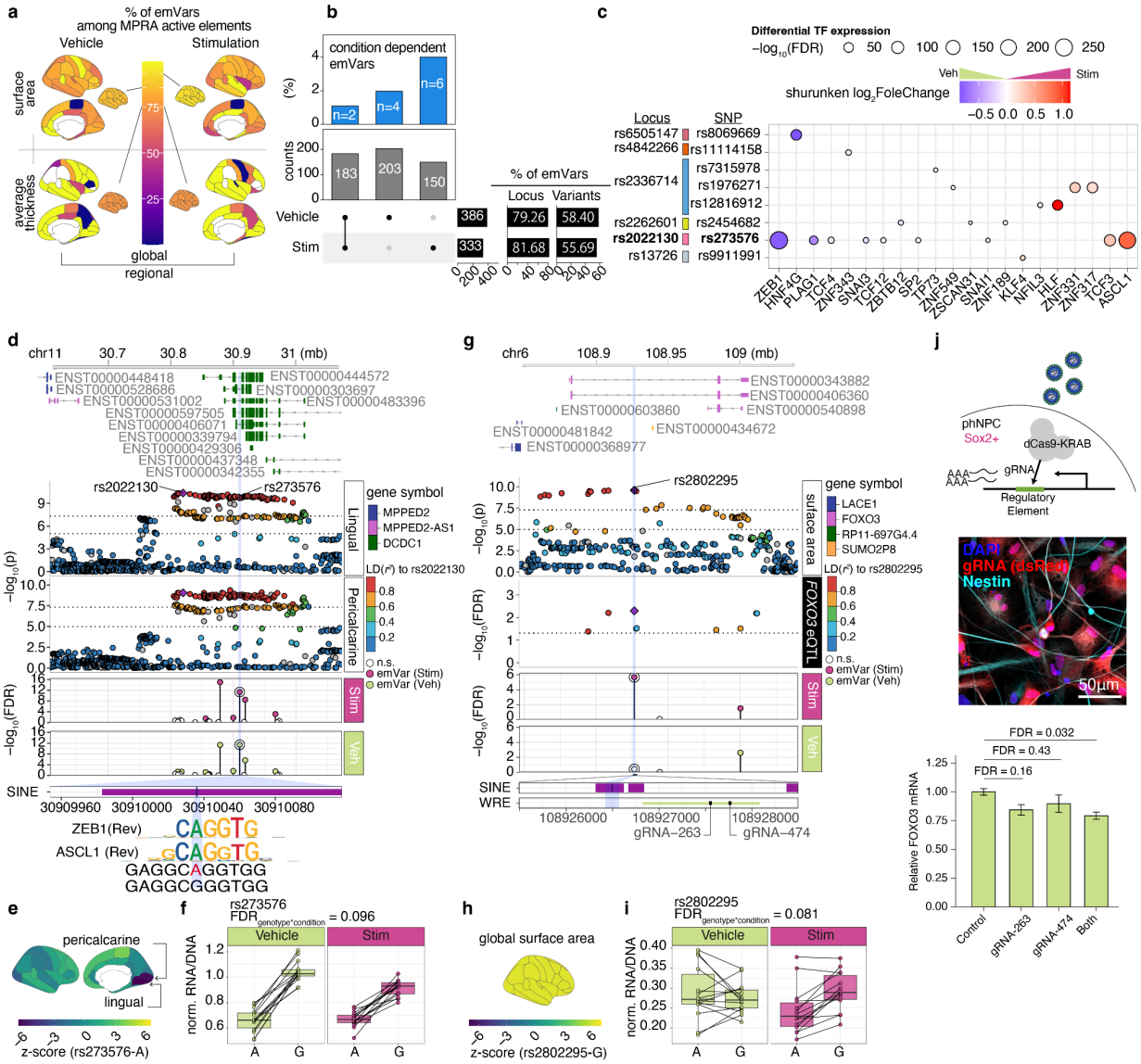

Fig. 6 Condition-dependent allelic effects in cortical structure associated regulatory elements

a, Percentage of emVar across brain regions stratified by condition (left = vehicle, right = stimulation) and measurements (surface area (top), thickness (bottom)). **b,** Number of emVars in each condition (bottom). The percentage of condition-dependent allelic effects (top). **c,** Disrupted TFs and their Wnt induced expression at condition-dependent allelic MPRA elements. The size of the dots indicates the significance of differential expression due to Wnt stimulation colored by shrunken $\log_2$FoldChange. **d**, *DCDC1* locus highlighting condition-dependent allelic MPRA element (rs273576). Top; -$\log_{10}$(pvalue) from GWAS of Lingual and Pericalcarine surface area. Each dot represents variants in the locus colored by LD (r^2) to the

index SNP (rs2022130, purple diamond). Middle: -$\log_{10}$(FDR) from MPRA activity in stimulation and vehicle conditions. Bottom: transposable elements and TFs disrupted by rs273576. **e**, Z score of GWAS regional surface area. **f,** Boxplot shows normalized RNA/DNA ratio of MPRA element (rs273576) stratified genotype and conditions. **g**, *FOXO3* locus highlighting condition-dependent allelic MPRA element (rs2802295) (left). Top: -$\log_{10}$(pvalue) from GWAS of global surface area and -$\log_{10}$(FDR) from *FOXO3* eQTL[48] (FDR < 0.05 are shown). Each dot represents variants in the locus colored by LD (r^2) to the index SNP (rs2802295, purple diamond). Middle: -$\log_{10}$(FDR) from MPRA allelic effects in stimulation and vehicle conditions. Bottom: transposable elements disrupted by rs2802295 and Wnt responsive element (WRE) and the position of the designed gRNAs for the CRISPRi experiment. **h**, Z score of GWAS global surface area. **i**, Boxplot shows normalized RNA/DNA ratio of MPRA element (rs2802295) stratified genotype and conditions. **j**, Experimental design of CRISPRi (top), immunofluorescence image showing expression of gRNA constructs in phNPCs (middle) and relative *FOXO3* expression as measured by qPCR (2 sample t-test with Holm post-hoc correction, n = 6 unique donors, mean+/- standard error are shown) (bottom).

Many variants (n = 183) showed MPRA allelic effects regardless of stimulation, but more variants were identified as emVars in only one condition (n_emVars$_{\text{stimulation only}}$ = 150, n_emVars$_{\text{vehicle only}}$ = 203), suggesting Wnt stimulation can drive condition-specific variant function (**Fig. 6a,b, Supplementary Table 3b,e**). By using an interaction test, we detected 12 variants with allelic effects that differ significantly across conditions (condition-dependent emVars) (**Fig. 6b**, **Supplementary Table 3f**). Of those, none disrupted TCF/LEF motifs which are TFs downstream of canonical Wnt pathway activation[49]. However, TFs disrupted by these stimulus-interacting SNPs were differentially expressed in phNPCs following Wnt stimulation, suggesting a mechanism by which cortical structure associated variants exert condition-specific allelic effects (**Fig. 6c**).

An interesting example of a condition-dependent emVar is rs273576 at the intron of *DCDC1*, where Wnt activation diminished the allelic effects detected in the MPRA (**Fig. 6c-f**). The A allele is associated with decreased lingual and pericalcarine surface areas and more closely matches binding sites for ZEB1 and ASCL1, TFs differentially expressed in response to Wnt stimulation[6] (**Fig. 6c,d**). This variant is an eQTL for *MPPED2* (300 kb downstream) in multiple tissues in GTEx, though not detected in brain or phNPCs.

Another example is rs2802295 within an intron of *FOXO3* (**Fig. 6g**). The G allele is associated with increased global surface area and decreased expression levels of *FOXO3* in the adult brain[48] (**Fig. 6g**). *FOXO3* gene expression was also downregulated under Wnt stimulation[6]. We detected an allelic effect at this variant under Wnt stimulation that was blunted in vehicle (**Fig. 6i**). This variant is proximal to a Wnt responsive element, where chromatin is less accessible due to Wnt stimulation. To validate the effects of this non-coding region on *FOXO3* gene expression, we

435 performed CRISPR interference (CRISPRi) by designing two gRNAs to target dCas9-KRAB
436 nearby this region (~1kb from rs2802295) (**Fig. 6j**). We found that silencing of this element by
437 dCas9-KRAB was associated with decreased expression of *FOXO3*, experimentally linking a
438 cortical surface area associated emVar to its gene of action. Using MPRA, CRISPRi validation,
439 and QTLs, we suggest a likely causal variant, gene, and context associated with differences in
440 human cortical structure.
441
442 In summary, we identified emVars associated with cortical structure. A subset of these variants
443 showed differential regulatory activity in response to Wnt stimulation, suggesting that signaling
444 pathways critical for brain development may influence the regulatory potential of the genetic
445 variants. These findings reveal how genetic variants shape cortical structure associated
446 differences in the human brain.
447

448 Discussion

449 Here, we assessed the gene regulatory potential of cortical structure associated variants in
450 phNPCs. We found that most cortical structure associated loci contained elements with regulatory
451 activity in phNPCs, and that cortical structure associated genetic variants influence the level of
452 that regulatory activity. Previous QTL studies using endogenous variation in populations of brain
453 tissue or phNPCs have also found that genetic variants exert effects during neural development
454 to influence adult cortical structure traits[4,6,50,51]. Our MPRA results provide further evidence to this
455 effect using experimental manipulation of alleles, ruling out confounding effects from other
456 variants that exist within an individual.
457
458 Because experimental manipulation allows the separation of alleles in high LD, specific genetic
459 variants can be nominated that alter gene regulatory function. Those variants that disrupt TF
460 binding motifs can be used to suggest TFs that lead to changes in cortical structure. Here, we
461 found that TFs like RARA, RARG, ZNF135, and NR2F1 are critical for determining inter-individual
462 differences in human cortical structure. Though previous work on these TFs has been conducted
463 in model systems like mice[52–54], our findings demonstrate that the TFs impact human brain
464 development and structure. We also propose a mechanism for region-specific effects detected in

465 cortical structure genetic association studies. The regional effects of variants correspond to the
466 expression levels of TFs that bind to them.
467
468 Wnt signaling has been well known in non-human model systems and in vitro human model
469 systems to impact brain development[19]. Therefore, we reasoned that the regulatory effect of
470 cortical structure associated variants may vary in response to Wnt stimulation. We find that
471 genetic variants exhibit Wnt stimulation-dependent gene regulatory function (**Fig. 5**), which we
472 have also demonstrated in the endogenous genome using chromatin accessibility and gene
473 expression[6]. Notably, genetic effects can be either accentuated or blunted due to Wnt stimulation.
474 This suggests that multiple cell types and stimulation states will need to be studied to fully
475 elucidate gene regulatory effects impacting cortical structure.
476
477 Alu elements are primate specific and have increased in prevalence in the genome coincident
478 with brain size increases along the human lineage[16]. Alu elements transcribe themselves through
479 highjacking proteins derived from other retrotransposable elements and insert themselves into
480 other regions of the genome, providing a mechanism for more rapid gene regulatory evolution
481 than the accumulation of single base pair mutations[15]. Here, we provide evidence that cortical
482 structure associated variants within Alu elements strongly influence transcription in phNPCs. This
483 suggests that Alu elements have been critical for creating gene regulatory elements that harbor
484 RARA, RARG, ZNF135, and NR2F1 motifs, which influence human cortical structure[41,42]. Over
485 time, these Alu elements have likely accumulated genetic variation that alters their function,
486 impacts gene expression during development, and contributes to inter-individual differences in
487 cortical structure.
488
489 We found that Pol III promoter regions supplied by Alu elements are strong drivers of MPRA
490 activity. Pol III is generally associated with transcription of short sequences, less than 500 bp in
491 length. Interestingly, the barcode element is contained within the 3' UTR of the luciferase gene
492 which is ~1.8 kb from the MPRA element, suggesting luciferase and the barcode are likely
493 transcribed by Pol II rather than Pol III. Given this evidence, we propose a mechanism whereby
494 Pol III transcribes the MPRA element, effectively forming an eRNA that enhances Pol II
495 recruitment, leading to higher expression of the luciferase gene and the barcode contained within.
496 This mechanism has in fact been observed in neural cells[14].
497

498 We implemented MPRA using transfection of episomal plasmids, so our results do not
499 recapitulate endogenous genome chromatinization, one of the major mechanisms underlying
500 gene regulation. Likely because of this, MPRA active elements had limited overlap with chromatin
501 accessibility peaks and MPRA allelic effects had limited overlap with caQTLs that were discovered
502 and replicated in the cell type (**Supplementary Fig. 1,5**). Nevertheless, a subset of MPRA active
503 elements did show overlap with eRNAs or uaRNAs active in phNPCs. Also, condition-dependent
504 MPRA elements showed evidence of mapping to genes with condition-dependent gene
505 expression. This provides evidence that MPRA active elements do have at least partial overlap
506 with activity in the endogenous genome. However, we cannot rule out that MPRA activity from
507 some elements is only due to episomal activity and gene regulatory activity from individual loci
508 would not be recapitulated within the endogenous genome[55]. Future studies generating specific
509 base pair edits in the endogenous genome would be able to disentangle these effects.

510 Methods

511 Ethics statement for human tissue-derived cell-lines

512 We acquired human fetal brain tissue following voluntary termination of pregnancy according to
513 IRB regulations at UCLA through the Gene and Cell Therapy Core after consent of the mother for
514 use of tissue in research. No compensation was provided to participants.

515 SNP Selection

516 Several variant sets were generated for inclusion in the MPRA. (1) *positive controls* - Known
517 promoter or enhancer sequences that are commonly used to constitutively drive gene expression
518 (minTk promoter, Ef1-alpha promoter, CMV promoter) were included. If the sequences were >150
519 bp, arbitrary 150 bp subsets were used. (2) *caQTLs* - SNPs within chromatin accessibility peaks
520 in primary human neural progenitors were selected for inclusion[4,6]. A 150 bp sequence
521 surrounding the variant from the human reference genome was included. Both alleles were
522 synthesized. Indels were removed. (3) *ENIGMA GWAS* - SNPs associated with human cortical
523 surface area or thickness were selected from a large GWAS of cortical surface area and
524 thickness[3]. Both alleles from all variants with $P < 1x10^{-5}$ in the association to a cortical structure
525 phenotype and $r^2 > 0.6$ to the identified index SNPs were included. A 150 bp sequence
526 surrounding the variant from the human reference genome was included. (4) *negative controls* -

527 Negative controls were generated by randomly scrambling the cortical structure associated
528 variant sequences for a subset of those variants. Each allele at the SNP of the unscrambled
529 sequence was included for analysis. Both alleles were removed when the MPRA library sequence
530 contained a restriction enzyme site used for cloning.

531 Creating variant oligo library

532 The 150 bp library oligos mentioned above were synthesized by Agilent and amplified via PCR
533 using the NEBNext 2X Q5 Hifi HS Mastermix (NEB, cat#M0453S) with primers MPRA-chipprimer-
534 R and MPRA-chipprimer-F. Primer information is available in **Supplementary Table 6.**
535
536 We then added random 20bp barcodes and restriction sequences (MluI and SpeI) to each variant
537 as previously described[22] using a pair of primers: MPRA-BC_Primer_R and MPRA-chipprimer-F.
538 Following library preparation, the sample was digested with SpeI-HF (NEB, cat#R3133S) and
539 MluI-HF (NEB, cat#R3198S) for 1 hour at 37°C. This step was immediately followed by a 1-hour
540 rSAP treatment (NEB, cat#M0371S) at 37°C, and then a 5-minute heat inactivation at 65°C.
541 Finally, the digested library was purified using the Zymo Clean and Concentrator Kit-5 (Zymo,
542 cat#D4033).

543 Creating MPRA Plasmid Library

544 The plasmid pJD_Donor_eGP2AP_RC was obtained from Addgene (Addgene, cat#133784). The
545 plasmid was digested with restriction enzymes SpeI-HF and MluI-HF for 1 hour at 37°C, then was
546 heat inactivated for 20 minutes at 80°C, brought to room temperature, followed by rSAP treatment
547 for 1 hour at 37°C, and heat inactivation for 5 minutes at 65°C. The digested plasmid was then
548 gel extracted from 1% agarose gel using Zymo Gel DNA Recovery kit (Zymo, cat#D4007). The
549 digested plasmid and oligo library was ligated together using T7 DNA ligase (NEB, cat#M0318S)
550 at room temperature for 30 minutes followed by clean up via Zymo clean and concentrator-5 kit.
551 The ligation product was transformed into NEB 5-alpha Electrocompetent E. coli (NEB, #C3020K),
552 grown for 7 hours at 30°C in 4L of LB, then maxi prepped using ZymoPURE II Plasmid Maxiprep
553 Kit (zymo, cat#D4203).

554 # Barcode Mapping

555 The barcodes (BC)s were mapped to the variants in a method previously described[22]. Briefly, the
556 barcode and variant region was amplified off the plasmid with primers that contain Illumina P5
557 and P7 adapters (*Bcmap_P5_AAV_R* and *Bcmap_P7_AAV_F_index*) with NEBNext 2X Q5 Hifi
558 HS Mastermix. The PCR product was purified and sequenced using the NovaSeq 6000 SP
559 (2×250 bp) with custom sequencing primers BCmap_R1Seq_AAV_R, BC_Map_R1seq, and
560 BCmap_R2Seq_AAV_F (**Supplementary Table 7**). The code used to map the barcodes to
561 variants can be found in this github repository: https://github.com/thewonlab/schizophrenia-
562 MPRA. There was a mean of 113 unique barcodes per variant prior to transfection.

563 # Adding in minimal promoter and Luciferase

564 The luciferase and minimal promoter sequences were obtained from the pGL4.23 plasmid
565 (Promega, cat#E841A). The pGL4.23 plasmid was enzymatically digested with KpnI-HF (NEB,
566 cat#R3142S) and XbaI (NEB, cat#R0145S) at 37°C for 3 hours, followed by heat inactivation at
567 65°C for 10 minutes. The digestion was cleaned up via Zymo clean and concentrator-5 kit, and
568 then gel extracted using Zymo Gel DNA Recovery kit, yielding a band size around 1.780Kb. The
569 plasmid containing the library and barcodes was digested first with KpnI-HF and rSAP at 37°C for
570 3 hours, then 65°C for 10 minutes for heat inactivation, cleaned up using Zymo clean and
571 concentrator-5 kit, and then gel extracted using Zymo Gel DNA Recovery kit. Then the product
572 was digested with XbaI and rSAP 37°C for 2 hours, then 65°C for 10 minutes for heat inactivation,
573 and cleaned up using Zymo clean and concentrator-5 kit. The digested plasmid containing the
574 library was ligated with the fragment carrying the minimal promoter and luciferase sequence using
575 T7 DNA ligase at room temperature for 30 minutes. The resulting construct was then purified with
576 the Zymo Clean and Concentrator-5 kit, yielding the final library plasmid, PJD_lib_minP_Luc.
577 PJD_lib_minP_Luc was transformed via heat shock into Library Efficiency DH5α Competent Cells
578 (Invitrogen, cat#18263012) and grown in kanamycin LB overnight at 30°C. The
579 PJD_lib_minP_Luc plasmid was maxi prepped with ZymoPURE II Plasmid Maxiprep Kit.

580 # Transfecting PJD_lib_minP_Luc into phNPCs

581 Acquisition of phNPCs and cell culture conditions were previously described[50]. Donor number 88
582 was used for these experiments and is biologically male. 6-well plates were coated with Poly-L-

583 Ornithine (10 µg/ml; Sigma-Aldrich, cat#P3655-100MG) and Laminin (10ug/mL, Corning,
584 cat#354232). After coating, phNPCs were plated at a concentration of 400,000 cells per well. The
585 cells were plated and fed with growth factors as described[22]. 24 hours after plating, the cells were
586 half fed with the media and growth factors described[22]. 48 hours after plating, the cells were half-
587 fed with the media and growth factors as described[22], and with nucleic acid transfection enhancer
588 (NATE) (1:100 final dilution; InvivoGen, cat#lyec-nate). 30 minutes after feeding, the cells were
589 transfected with PJD_lib_minP_Luc plasmid via Lipofectamine Stem Transfection Reagent
590 (Invitrogen, cat#STEM00001) according to the instructions, using Opti-Mem (Thermo Scientific,
591 cat#31985070), 2.5ug of PJD_lib_minP_Luc plasmid, and 1ug of pUC19 plasmid (Thermo
592 Scientific, cat#SD0061) per single 6-well. Co-transfecting with pUC19 plasmid increased
593 transfection efficiency. 24 hours after transfection, the cells were half fed and then treated either
594 with 7uL of 2.5uM CHIR or 7uL DMSO (vehicle). At exactly 48 hours after CHIR or vehicle
595 treatment, RNA and DNA was extracted from the cells using the Quick-DNA/RNA Miniprep Plus
596 Kit (Zymo, cat#D7003), with 600 µL of Shield Buffer and 600 µL of Lysis Buffer per well. In total,
597 there were 16 vehicle replicates and 16 CHIR replicates, where one replicate was one well in a
598 6-well plate. For each 6-well plate, three wells were vehicle and three wells were CHIR treated.

599 MPRA Library Preparation For Sequencing

600 Extracted RNA was reverse-transcribed into cDNA using SuperScript IV Reverse Transcriptase
601 (Invitrogen, cat. no. 18090050) and a primer designed to bind downstream of the barcodes
602 (Lib_Hand_RT). The resulting cDNA was then amplified with Lib_Hand and Lib_seq_Luc_R
603 primers, utilizing NEBNext 2X Q5 Hifi HS Mastermix, and then purified using the Zymo DNA Clean
604 and Concentrator kit-25 (Zymo, cat. no. D4033).

605 Additionally, 4 µL of DNA from each well was PCR amplified in four separate PCR reactions using
606 Lib_Hand_RT and Lib_Seq_Luc_R primers with NEBNext 2X Q5 Hifi HS Mastermix, followed by
607 purification with the Zymo Clean and Concentrator kit-25. P5 and P7 adapter sequences and i7
608 demultiplexing indices were then incorporated into both cDNA and DNA libraries through PCR
609 using P5_seq_Luc_F and P7_Ind_#_Han primers with NEBNext 2X Q5 Hifi HS Mastermix.

610 The final PCR products were purified and size-selected using AMPure XP Beads (Beckman
611 Coulter, cat. no. A63881) at 0.7X and 0.9X ratios to isolate a 273 bp DNA fragment. The libraries
612 were then sequenced on a NovaSeq SP using a 35 × 8 × 0 cycle format with 20% PhiX and
613 custom sequencing primers Index_primer and R1_primer (**Supplementary Table 8**).

614 # MPRA data processing

615 Sequencing alignment and Quantification of barcode counts: Adapter sequences were trimmed
616 using cutadapt (v4.1)[56] using default parameters. Trimmed sequences were then converted to
617 reverse complement DNA sequences. We extracted only sequences with 20 bp length and
618 perfectly matched to the BC information in the barcode-variant table which consists of the unique
619 barcode-variant pairs.
620
621 In each replicate, we first filtered BCs if the DNA and RNA read counts had less than 5 read
622 counts, and kept elements with at least 5 unique BC. Per each variant and replicate,
623 $\log_2$(RNA/DNA) were fed to boxplot.stats() to detect BC outliers (**Supplementary Fig. 2)**. After
624 removing BC outliers, RNA and DNA counts were combined for each element. Among 16
625 replicates, those with lower correlation to other biological replicates (correlation coefficients to
626 others = 0.3 - 0.7) were removed. Elements available at least 10 replicates were retained for
627 analysis.
628

629 # MPRA regulatory effects

630 Regulatory activity: For each dataset (caQTL, ENIGMA-vehicle, ENIGMA-stimulation), α values
631 (transcription rate adjusted by batch effects including sequencing depth) were estimated using
632 *analyzeQuantification()* implemented in MPRAnalyze(v1.9.1)[57] to assess regulatory activity of
633 each element compared to the distribution of background (α of negative controls). *P*-values of
634 median absolute deviation score (*P*-MAD score) were corrected for multiple comparisons by the
635 Benjamini-Hochberg (BH) procedure [FDR]. Condition-dependent MPRA elements were
636 identified among MPRA elements that were available in both conditions and were active in at least
637 one of the conditions. Differential activity was estimated using *analyzeComparative()* followed by
638 *testLtr()* in MPRAnalyze. For this analysis we excluded one replicate that had library size
639 correction factors of DNA < 0.10 which led to the failure to execute *analyzeComparative()*. We set
640 a statistical significant threshold at FDR < 0.1 to define "Active" elements or condition-dependent
641 elements. In most subsequent analyses including enrichment analyses, each region was
642 classified if either allele exhibited MPRA activity and as inactive if both alleles showed no
643 detectable activity to ensure that each region was counted only once.
644

645 Allelic effect: We applied *mpralm()* (mpra v.1.16.0)[58] followed by *topTable()* (limma v3.50.3)[59] to
646 detect allelic effects in MPRA active elements (MPRA element pairs with one of element was
647 active in any conditions). Condition-dependent allelic effects were assessed with
648 ~genotype+condition+genotype*condition. Only MPRA element pairs that showed allelic
649 differences (emVars) in at least one condition were used to test for condition-dependent effects.
650 We set a statistical significance threshold at FDR < 0.1 to define emVars or condition-dependent
651 emVars.
652

653 # Transposable elements

654 Transposable elements (TEs) overlapping MPRA elements were annotated using the
655 RepeatMasker database obtained from the UCSC Table Browser. SINE, LINE, or LTR classes
656 were extracted since those had at least 500 regions overlapped with MPRA elements used in this
657 study (1,825, 1,367, 746, respectively). Alu elements, a subclass of SINEs, were further classified
658 into three groups based on milliDiv score (<100, 100-150, >150)[35] to interpret evolutionary ages.
659
660 Relative position of MPRA elements within the Alu sequence: To estimate the position of the
661 MPRA element within the Alu element, the genomic location of each MPRA element was identified
662 and overlapped with forward oriented Alu element that had length ≥ 250 bp. This position was
663 used to estimate the approximate location of the A-Box (TGGCTCACGCC) and the B-Box
664 (GTTCGAGAC), A_5TACA_6, and the poly-A Tail[33,34]. The relative MPRA element position within the
665 Alu was determined by the distance from the Alu start position to the midpoint of the overlapping
666 regions.
667
668 Enrichment analysis: Fisher's exact tests were performed to assess the following enrichment of
669 RE features in target groups against specified background.
670 (1) Frequency of each TE overlaps (active vs inactive), (2) frequency of Alu overlaps (SINE-active
671 vs SINE-inactive), (3) frequency of forwarded oriented Alu (Alu-active vs Alu-inactive), (4)
672 frequency of A/B box followed by TTTT in 150bp, and (5) frequency of emVars in Alu elements
673 (emVars vs MPRA active elements with non significant allelic effects).
674

675 When we tested enrichment in stimulation-enhancing MPRA activity, we used the number of RE
676 in MPRA elements with non-significant activity differences between conditions as a reference
677 while running Fisher's exact test. We considered significant enrichment if FDR < 0.1.

678 TF binding site motif enrichment test

679 To avoid testing redundant TF binding site [TFBS] motifs[60], we used pre-clustered TF bind motifs
680 available in JASPAR website
681 (https://jaspar2020.genereg.net/static/clustering/2020/vertebrates/CORE/interactive_trees/JASP
682 AR_2020_matrix_clustering_vertebrates_archive.zip]. Among 137 clusters, we extracted clusters
683 in which at least one TF was expressed in phNPCs in either Vehicle or Wnt-stimulated condition[6],
684 resulting in 123 clusters. TFBSs within the 150 bp MPRA elements were predicted by FIMO
685 (v5.5.2)[61] with FDR < 0.1.
686 We evaluated (1) enrichment for any TF clusters overlaps, and (2) specific TF clusters using
687 Fisher's exact test.

688 Enrichment analysis in various features for MPRA active elements

689 Since we tested MPRA activity per element not per variant, we extracted one element per variant
690 with higher activity (i.e. smaller *P* value) for enrichment analyses unless specified. Those
691 elements were then grouped as either active elements (FDR < 0.1) or inactive elements (FDR ≥
692 0.1). In the inactive group, we ensured that both elements were tested and inactive. Two-tailed
693 Fisher's Exact tests were used to estimate the enrichment or depletion of MPRA active elements
694 using MPRA inactive elements as a background set unless specified in the section below. A
695 threshold of FDR < 0.1 was applied to identify statistically significant results.

696 MPRA elements regulating their putative target genes

697 Endogenous gene regulatory information: Data were acquired from our previous study[6]. Protein-
698 coding genes or lincRNAs expressed in unstimulated (vehicle) or CHIR stimulated phNPCs were

699 extracted. Differentially expressed genes (DEGs) and differentially accessible chromatin peaks
700 due to CHIR stimulation were defined if FDR < 0.1.
701
702 Mapping MPRA element to genes: We mapped MPRA elements to genes by overlapping either
703 promoter regions defined as 2kb upstream of transcription start site (TSS) in Gencode v19 or
704 chromatin interaction (Hi-C loops) from germinal zone (GZ) or cortical plate (CP). The proportion
705 of MPRA elements linked to their putative target genes were compared between MPRA active
706 elements vs MPRA inactive elements using Fisher's exact test.
707
708 Directionality of condition-dependent effect: *binom.test()* was applied to test whether the
709 percentage of concordant directionality of effect between MPRA activity and gene expression due
710 to Wnt stimulation was higher than expected by chance.

711 Prediction of TFs disrupted by emVars

712 motifbreakR (v2.8.0)[62] were used to predict TFs disrupted by emVars on JASPAR2022 vertebrate
713 from MotifDB with method='ic', threshold = 1e-4. We further extracted TFs predicted as strongly
714 impacted (effect= "strong") by motifBreakR and expressed in unstimulated and/or stimulated
715 condition in phNPCs.

716 CRISPRi experiments

717 gRNAs targeting a putative regulatory element near rs2802295 were designed using GT-Scan[63]
718 for CRISPRi experiments. An initial 4 targeting gRNAs positioned at roughly even spacing along
719 the length of the regulatory element were selected in addition to 2 non-targeting gRNAs as
720 controls. All gRNAs sequences tested are listed in **Supplementary Table 9** with the ones used
721 for statistical analyses and high content screening in bold. gRNAs were cloned into pLV-U6-C-
722 UbC-DsRed-P2A-Bsr (https://www.addgene.org/83919/) for gene expression experiments. Lenti-
723 dCas9-KRAB-blast (https://www.addgene.org/89567/) vector was used for dCas9-KRAB
724 expression. Lentiviruses for each plasmid were generated using the psPax2
725 (https://www.addgene.org/12260/) packaging plasmid and pMD2.G
726 (https://www.addgene.org/12259/) envelope plasmid as described previously[5]. 293T cells were
727 cultured directly in phNPC proliferation media for 48 hours after transfection using TransIT-LT1
728 Transfection Reagent (Mirus Bio). The viral supernatant was then harvested, purified by syringe

729 filtering, and frozen at -80°C for direct use in subsequent experiments. Viral titers were calculated
730 using the qPCR Lentivirus Titer Kit (Applied Biological Materials). A preliminary screen of the 4
731 gRNAs was performed to identify those with the highest potential for perturbing *FOXO3*
732 expression. phNPCs were plated in 24 well plates at 80,000 cells per well. The following day, cells
733 were infected with viruses for Lenti-dCas9-KRAB-blast and pLV-U6-C-UbC-DsRed-P2A-Bsr
734 containing the targeting gRNAs at a calculated MOI of 2 for each virus. Plates were then spun at
735 37°C for 1 hour to increase transduction efficiency[64]. phNPCs were cultured for an additional 5
736 days after infection prior to RNA extraction.
737
738 RNA purification was performed using the Direct-Zol RNA Microprep Kit (Zymo Research) and
739 cDNA from 200ng of purified RNA was generated using the iScript cDNA Synthesis Kit (Bio-Rad).
740 Gene expression was then measured by qPCR using the SsoAdvanced Universal SYBR Green
741 Supermix (Bio-Rad) and a QuantStudio 5 Real-Time PCR System (Thermo Fisher). *FOXO3*
742 expression was normalized to the expression of the *ACTB* (Beta-actin) gene. Gene expression
743 values for each targeting gRNA were compared to the average of the non-targeting controls.
744 Primers used for qPCR are provided in **Supplementary Table 10.**
745
746 From our initial pilot screen, the 2 gRNAs out of 4 with the highest impact on gene expression
747 were used for downstream experiments. qPCR experiments for each individual gRNA or a
748 combination of 2 gRNAs were repeated for 5-6 unique phNPC donor lines with the average
749 expression of 3 wells per donor per gRNA combination considered a biological replicate.

750 Correlation between regional TF expression and GWAS SNP
751 effects

752 Normalized gene expressions in fetal brains (8 post-conception weeks (pcw) to 24 pcw) were
753 obtained from BrainSpan Atlas of the Developing Human Brain
754 https://www.brainspan.org/static/download.html[65]. Gene expression was averaged for each
755 cortical region defined by Allen Human Brain Atlas (AHBA) (**Supplementary Fig. 8**). GWAS Z
756 scores were calculated using the effect size of the allele that matched the TF motif sequence
757 divided by the standard error. Since brain regions used within the ENIGMA GWAS were based
758 on Desikan-Killiany Atlas (DK-Atlas), we mapped 36 DK regions to 16 AHBA regions for
759 comparison. Linear regression was used to assess correlation between GWAS Z score and gene
760 expressions.

Data availability

Data generated in this study are provided as supplementary tables, and raw data will be available upon publication.

Code availability

All code used in analyses will be available before publication.

Author Contributions

H.W. and J.L.S. conceived and supervised the study, and together with N.M., J.C.M., designed the study and data analysis strategy. J.C.M., O.K, and J.B. performed MPRA. N.M. conducted computational analyses. O.K. performed and analyzed CRISPRi experiment. B.D.L and J.M.V. provided Wnt dependent gene regulatory data. N.M., J.C.M., G.E.C., H.W. and J.L.S. interpreted the results. N.M., J.C.M, H.W., and J.L.S. wrote the initial draft of the manuscript. All co-authors provided critical feedback and approved the manuscript.

References

1. Sousa, A. M. M., Meyer, K. A., Santpere, G., Gulden, F. O. & Sestan, N. Evolution of the Human Nervous System Function, Structure, and Development. *Cell* **170**, 226–247 (2017).
2. Geschwind, D. H. & Rakic, P. Cortical evolution: judge the brain by its cover. *Neuron* **80**, 633–647 (2013).
3. Grasby, K. L. *et al.* The genetic architecture of the human cerebral cortex. *Science* **367**, (2020).
4. Liang, D. *et al.* Cell-type-specific effects of genetic variation on chromatin accessibility during human neuronal differentiation. *Nat. Neurosci.* (2021) doi:10.1038/s41593-021-00858-w.

785 5. de la Torre-Ubieta, L. *et al.* The Dynamic Landscape of Open Chromatin during Human
786 Cortical Neurogenesis. *Cell* **172**, 289-304.e18 (2018).
787 6. Matoba, N. *et al.* Stimulating Wnt signaling reveals context-dependent genetic effects on
788 gene regulation in primary human neural progenitors. *Nat. Neurosci.* (2024)
789 doi:10.1038/s41593-024-01773-6.
790 7. Bhaduri, A. *et al.* An atlas of cortical arealization identifies dynamic molecular signatures.
791 *Nature* **598**, 200–204 (2021).
792 8. Chenn, A. & Walsh, C. A. Regulation of cerebral cortical size by control of cell cycle exit in
793 neural precursors. *Science* **297**, 365–369 (2002).
794 9. Gasperini, M., Tome, J. M. & Shendure, J. Towards a comprehensive catalogue of
795 validated and target-linked human enhancers. *Nat. Rev. Genet.* **21**, 292–310 (2020).
796 10. Won, H. *et al.* Chromosome conformation elucidates regulatory relationships in developing
797 human brain. *Nature* **538**, 523–527 (2016).
798 11. Hu, B. *et al.* Neuronal and glial 3D chromatin architecture informs the cellular etiology of
799 brain disorders. *Nat. Commun.* **12**, 3968 (2021).
800 12. Sey, N. Y. A. *et al.* A computational tool (H-MAGMA) for improved prediction of brain-
801 disorder risk genes by incorporating brain chromatin interaction profiles. *Nat. Neurosci.* **23**,
802 583–593 (2020).
803 13. Liang, L. *et al.* Complementary Alu sequences mediate enhancer-promoter selectivity.
804 *Nature* **619**, 868–875 (2023).
805 14. Policarpi, C. *et al.* Enhancer SINEs link Pol III to Pol II transcription in neurons. *Cell Rep.*
806 **21**, 2879–2894 (2017).
807 15. Fueyo, R., Judd, J., Feschotte, C. & Wysocka, J. Roles of transposable elements in the
808 regulation of mammalian transcription. *Nat. Rev. Mol. Cell Biol.* **23**, 481–497 (2022).
809 16. Wang, J., Weatheritt, R. & Voineagu, I. Alu-minating the mechanisms underlying primate
810 cortex evolution. *Biol. Psychiatry* **92**, 760–771 (2022).

811 17. McAfee, J. C. *et al.* Focus on your locus with a massively parallel reporter assay. *J.*
812 *Neurodev. Disord.* **14**, 50 (2022).
813 18. Degner, K. N., Bell, J. L., Jones, S. D. & Won, H. Just a SNP away: The future of in vivo
814 massively parallel reporter assay. *Cell Insight* **4**, 100214 (2024).
815 19. Harrison-Uy, S. J. & Pleasure, S. J. Wnt signaling and forebrain development. *Cold Spring*
816 *Harb. Perspect. Biol.* **4**, a008094 (2012).
817 20. Lee, S. *et al.* Massively parallel reporter assay investigates shared genetic variants of eight
818 psychiatric disorders. *Cell* **0**, (2025).
819 21. Bain, J. *et al.* The selectivity of protein kinase inhibitors: a further update. *Biochem. J* **408**,
820 297–315 (2007).
821 22. McAfee, J. C. *et al.* Systematic investigation of allelic regulatory activity of schizophrenia-
822 associated common variants. *Cell Genom.* **3**, 100404 (2023).
823 23. Abell, N. S. *et al.* Multiple causal variants underlie genetic associations in humans. *Science*
824 **375**, 1247–1254 (2022).
825 24. Deng, C. *et al.* Massively parallel characterization of regulatory elements in the developing
826 human cortex. *Science* **384**, eadh0559 (2024).
827 25. Siraj, L. *et al.* Functional dissection of complex and molecular trait variants at single
828 nucleotide resolution. *bioRxiv* (2024) doi:10.1101/2024.05.05.592437.
829 26. Zeng, B. *et al.* Genetic regulation of cell type-specific chromatin accessibility shapes brain
830 disease etiology. *Science* **384**, eadh4265 (2024).
831 27. Khetan, S. *et al.* Functional characterization of T2D-associated SNP effects on baseline
832 and ER stress-responsive β cell transcriptional activation. *Nat. Commun.* **12**, 5242 (2021).
833 28. Stefansson, H. *et al.* A common inversion under selection in Europeans. *Nat. Genet.* **37**,
834 129–137 (2005).
835 29. Oliveros, W. *et al.* Systematic characterization of regulatory variants of blood pressure
836 genes. *Cell Genom.* **3**, 100330 (2023).

837 30. Erwin, J. A., Marchetto, M. C. & Gage, F. H. Mobile DNA elements in the generation of
838 diversity and complexity in the brain. *Nat. Rev. Neurosci.* **15**, 497–506 (2014).
839 31. Deininger, P. Alu elements: know the SINEs. *Genome Biol.* **12**, 236 (2011).
840 32. Roberts, B. S. *et al.* Genome-wide strand asymmetry in massively parallel reporter activity
841 favors genic strands. *Genome Res.* **31**, 866–876 (2021).
842 33. Paolella, G., Lucero, M. A., Murphy, M. H. & Baralle, F. E. The Alu family repeat promoter
843 has a tRNA-like bipartite structure. *EMBO J.* **2**, 691–696 (1983).
844 34. Conti, A. *et al.* Identification of RNA polymerase III-transcribed Alu loci by computational
845 screening of RNA-Seq data. *Nucleic Acids Res.* **43**, 817–835 (2015).
846 35. Smit, AFA, Hubley, R. & Green, P. *RepeatMasker Open-4.0*.
847 <http://www.repeatmasker.org> (2013-2015).
848 36. Shannon, C. E. A mathematical theory of communication. *Bell Syst. Tech. J.* **27**, 379–423
849 (1948).
850 37. Cooper, Y. A. *et al.* Functional regulatory variants implicate distinct transcriptional networks
851 in dementia. *Science* **377**, eabi8654 (2022).
852 38. Zhou, B., He, Y., Chen, Y. & Su, B. Comparative Genomic Analysis Identifies Great-Ape-
853 Specific Structural Variants and Their Evolutionary Relevance. *Mol. Biol. Evol.* **40**, (2023).
854 39. Li, H. *et al.* Transcription factor MEF2C influences neural stem/progenitor cell differentiation
855 and maturation *in vivo*. *Proc. Natl. Acad. Sci. U. S. A.* **105**, 9397–9402 (2008).
856 40. Harrington, A. J. *et al.* MEF2C regulates cortical inhibitory and excitatory synapses and
857 behaviors relevant to neurodevelopmental disorders. *Elife* **5**, (2016).
858 41. Osipovich, A. B. *et al.* ZFP92, a KRAB domain zinc finger protein enriched in pancreatic
859 islets, binds to B1/Alu SINE transposable elements and regulates retroelements and genes.
860 *PLoS Genet.* **19**, e1010729 (2023).
861 42. Hansen, T. J., Fong, S. L., Day, J. K., Capra, J. A. & Hodges, E. Human gene regulatory
862 evolution is driven by the divergence of regulatory element function in both cis and trans.

863 *Cell Genom.* **4**, 100536 (2024).
864 43. Vansant, G. & Reynolds, W. F. The consensus sequence of a major Alu subfamily contains
865 a functional retinoic acid response element. *Proc. Natl. Acad. Sci. U. S. A.* **92**, 8229–8233
866 (1995).
867 44. Naqvi, S. *et al.* Precise modulation of transcription factor levels identifies features
868 underlying dosage sensitivity. *Nat. Genet.* **55**, 841–851 (2023).
869 45. Domingo, J. *et al.* Non-linear transcriptional responses to gradual modulation of
870 transcription factor dosage. *bioRxiv* (2024) doi:10.1101/2024.03.01.582837.
871 46. Miller, J. A. *et al.* Transcriptional landscape of the prenatal human brain. *Nature* **508**, 199–
872 206 (2014).
873 47. Calvo, F. *et al.* Cdc42EP3/BORG2 and Septin Network Enables Mechano-transduction and
874 the Emergence of Cancer-Associated Fibroblasts. *Cell Rep.* **13**, 2699–2714 (2015).
875 48. Wang, D. *et al.* Comprehensive functional genomic resource and integrative model for the
876 human brain. *Science* **362**, (2018).
877 49. Cadigan, K. M. & Waterman, M. L. TCF/LEFs and Wnt signaling in the nucleus. *Cold Spring*
878 *Harb. Perspect. Biol.* **4**, a007906–a007906 (2012).
879 50. Aygün, N. *et al.* Brain-trait-associated variants impact cell-type-specific gene regulation
880 during neurogenesis. *Am. J. Hum. Genet.* **108**, 1647–1668 (2021).
881 51. Walker, R. L. *et al.* Genetic Control of Expression and Splicing in Developing Human Brain
882 Informs Disease Mechanisms. *Cell* **179**, 750-771.e22 (2019).
883 52. Shibata, M. *et al.* Regulation of prefrontal patterning and connectivity by retinoic acid.
884 *Nature* **598**, 483–488 (2021).
885 53. Liu, Z. *et al.* Nr2f1 enhancers have distinct functions in controlling Nr2f1 expression during
886 cortical development. *Proc. Natl. Acad. Sci. U. S. A.* **121**, e2402368121 (2024).
887 54. Grove, E. A. Area patterning of the mammalian neocortex. in *Patterning and Cell Type*
888 *Specification in the Developing CNS and PNS* 49–68 (Elsevier, 2020).

889 55. Englander, E. W., Wolffe, A. P. & Howard, B. H. Nucleosome interactions with a human Alu
890 element. Transcriptional repression and effects of template methylation. *J. Biol. Chem.* **268**,
891 19565–19573 (1993).
892 56. Martin, M. Cutadapt removes adapter sequences from high-throughput sequencing reads.
893 *EMBnet J.* **17**, 10 (2011).
894 57. Ashuach, T. *et al.* MPRAnalyze: statistical framework for massively parallel reporter assays.
895 *Genome Biol.* **20**, 183 (2019).
896 58. Myint, L., Avramopoulos, D. G., Goff, L. A. & Hansen, K. D. Linear models enable powerful
897 differential activity analysis in massively parallel reporter assays. *BMC Genomics* **20**, 209
898 (2019).
899 59. Ritchie, M. E. *et al.* limma powers differential expression analyses for RNA-sequencing and
900 microarray studies. *Nucleic Acids Res.* **43**, e47 (2015).
901 60. Castro-Mondragon, J. A., Jaeger, S., Thieffry, D., Thomas-Chollier, M. & van Helden, J.
902 RSAT matrix-clustering: dynamic exploration and redundancy reduction of transcription
903 factor binding motif collections. *Nucleic Acids Res.* **45**, e119–e119 (2017).
904 61. Grant, C. E., Bailey, T. L. & Noble, W. S. FIMO: scanning for occurrences of a given motif.
905 *Bioinformatics* **27**, 1017–1018 (2011).
906 62. Coetzee, S. G., Coetzee, G. A. & Hazelett, D. J. motifbreakR: an R/Bioconductor package
907 for predicting variant effects at transcription factor binding sites. *Bioinformatics* **31**, 3847–
908 3849 (2015).
909 63. O'Brien, A. & Bailey, T. L. GT-Scan: identifying unique genomic targets. *Bioinformatics* **30**,
910 2673–2675 (2014).
911 64. Topol, A., Tran, N. N. & Brennand, K. J. A guide to generating and using hiPSC derived
912 NPCs for the study of neurological diseases. *J. Vis. Exp.* e52495 (2015).
913 65. BrainSpan Atlas of the Developing Human Brain. http://brainspan.org (2011).

Acknowledgements

This research was supported by the PsychENCODE consortium (R01MH122509, H.W. and J.L.S.). We acknowledge the technical support from the UNC High Throughput Sequencing Facility (HTSF; University Cancer Research Fund; Comprehensive Cancer Center Core Support grant, P30CA016086; UNC Center for Mental Health and Susceptibility grant, P30ES010126). We would like to acknowledge the use of bioRender (www.biorender.com) templates to make the cartoon in Fig. 1.